JOURNAL OF GUIDANCE, CONTROL, AND DYNAMICS
Vol. 15, No. 2, March-April 1992

Adaptive Control Applied to Momentum Unloading Using the Low Earth Orbital Environment

T. F. Burns*
TRW, Inc., Redondo Beach, California 90089
and
H. Flashner†
University of Southern California, Los Angeles, California 90278

An adaptive control technique for the unloading of spacecraft angular momentum is presented. The technique employs model reference adaptive control theory with Lyapunov stability analysis to synthesize a controller using multiple environmental sources in combination for unloading. Simulation studies are presented that employ magnetic, gravity gradient, and aerodynamic torques in a three-way controller. It is shown that momentum is contained within a dead zone introduced for disturbance compensation that is well below reasonable reaction wheel saturation limits for two model spacecraft of much different mass properties.

Introduction

MANY momentum management schemes employ the interaction of the spacecraft with the low Earth orbit environment to generate the needed unloading torques. This study presents a scheme for spacecraft momentum management that uses the three environmental sources of magnetics, gravity gradient, and aerodynamics. It is directed at three-axis stabilized vehicles possessing angular momentum storage devices such as reaction wheels. The scheme employs an adaptive control approach to the problem.

Gravity gradient torques have been suggested for the development of a torque equilibrium attitude (TEA) control scheme for the proposed NASA Space Station.[1,2] Magnetic torquing applied to desaturation of momentum storage devices has been implemented on, or is proposed for, many spacecraft programs. It usually involves the cross product unloading law, the minimum energy desaturation law, or more simple bang-bang laws.[3,4]

The application of adaptive control by means of augmenting the control system state with system parameters has not yet been applied to momentum unloading. The concept of having self-tuning system parameters is appealing when the external perturbations affecting momentum unloading systems are considered, such as geomagnetic storms and atmospheric density variations. For an Earth-pointing spacecraft in a low circular orbit, the combination of the three unloading methods employed in this study allows the ready accommodation of the limitations of each method taken individually. For example, gravity gradient unloading cannot reduce momentum in the Earth-pointing direction, and magnetic unloading cannot reduce momentum in the instantaneous magnetic field direction. However, when they are used together, all three momentum components can be reduced.

This study applies adaptive control in its model reference form. Model reference adaptive control (MRAC) allows the designer to choose an asymptotically stable reference model whose behavior the output or state of the system is forced to follow. Porter and Tatnall[5] derived such a system focusing on control of the state. Since then, a large variety of work has been published on model reference control of the system output,[6] analysis of adaptive parameter boundedness,[7] and robustness issues.[8]

This paper is organized into five sections. The second section covers the fundamental momentum unloading problem. The adaptive unloading scheme of this study is presented in the third section. The stability of the method is analyzed, and its implementation in simulation is discussed for two model spacecraft using combinations of magnetic, gravity gradient, and aerodynamic unloading. Simulation results are presented in the fourth section, and concluding remarks are presented thereafter.

Momentum Unloading Problem

The approach taken for unloading control here is to consider the momentum unloading control system (MUCS) control torques as perturbations to the attitude control system (ACS), and vice versa (see Fig. 1). This design approach for the two loops is often employed,[9] justified by the difference in bandwidths between ACS and MUCS. The attitude control system has a time constant on the order of seconds to minutes; the momentum control is on a scale of minutes or possibly hours. In a three-axis stabilized, Earth-pointing spacecraft, assuming perfect attitude control, total angular momentum $\Delta\mathfrak{H}$ equals the change in angular momentum of the reaction wheels, $\Delta \boldsymbol{H}$ in body frame.

Magnetic Unloading

A magnetic moment $\boldsymbol{M}$ generated via electromagnets on board the spacecraft causes a torque $\boldsymbol{T}_M$ given in body frame by:

$$\boldsymbol{T}_M = \boldsymbol{M} \times \boldsymbol{B} \tag{1}$$

where $\boldsymbol{B}$ is the Earth's magnetic field vector.

We adopt a matrix notation in which a vector $\boldsymbol{V} = V_x\hat{i} + V_y\hat{j} + V_z\hat{k}$ is denoted by a column matrix $V = [V_x\ V_y\ V_z]^T$. Then Eq. (1) can be written as

$$T_M = \underline{B}M \tag{2}$$

where $M = [M_x\ M_y\ M_z]^T$ and

$$\underline{B} = \begin{bmatrix} 0 & B_z & -B_y \\ -B_z & 0 & B_x \\ B_y & -B_x & 0 \end{bmatrix}$$

Presented as Paper 89-3472 at the AIAA Guidance, Navigation, and Control Conference, Boston, MA, Aug. 14-16, 1989; received Oct. 18, 1989; revision received Oct. 8, 1990; accepted for publication Oct. 22, 1990.

*Member of Technical Staff, Space and Technology Group. Member AIAA.

†Assistant Professor, Department of Mechanical Engineering. Member AIAA.

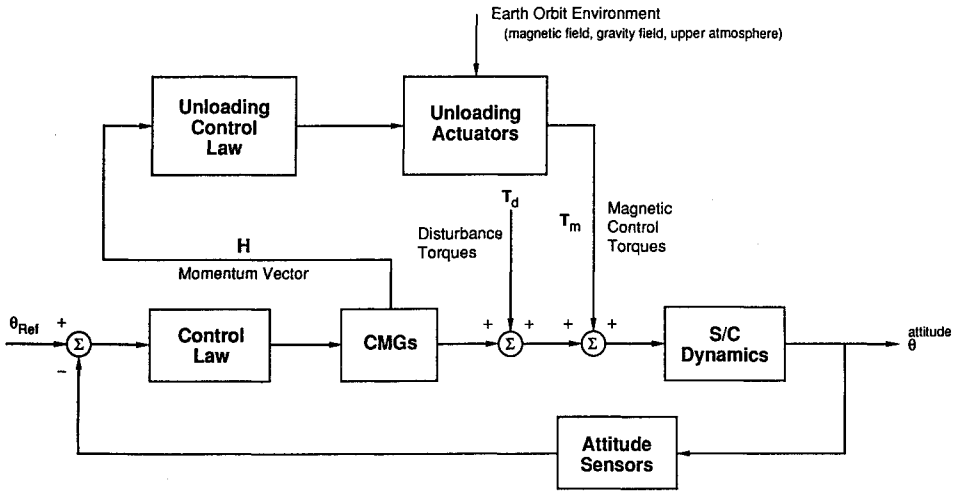

Fig. 1 Attitude and momentum unloading control systems.

Gravity Gradient Unloading

Perturbation torques arising from the effect of the Earth's gravitational field on an asymmetrical spacecraft body may be used to the ACS designer's advantage by incorporating them into a momentum unloading scheme. Let us assume that the Earth-pointing unit vector is aligned with the body z axis and that the spacecraft attitude configuration is Earth pointing, such that the attitude angles roll ϕ, pitch θ, and yaw ψ are small ($\pm$ 10 deg) rotations from the orbit reference frame to the spacecraft body frame. Then gravity gradient control torque can be expressed as:

$$T_{Gx} = (3\mu/R_c^3)(I_{zz}-I_{yy})\phi$$

$$T_{Gy} = (3\mu/R_c^3)(I_{zz}-I_{xx})\theta$$

$$T_{Gz} = 0 \tag{3}$$

where μ is the Earth gravitational constant; R_c is the distance from the Earth's center to spacecraft's center of mass; I_{xx}, I_{yy}, and I_{zz} are the body principal moments of inertia; and ϕ and θ are control inputs. In matrix notation, Eq. (3) can be written as

$$T_G = \underline{G}\Phi \tag{4}$$

where $\Phi = [\phi\ \theta]^T$ and

$$\underline{G} = \begin{bmatrix} I_{zz}-I_{yy} & 0 \\ 0 & I_{zz}-I_{xx} \\ 0 & 0 \end{bmatrix}$$

Aerodynamic Unloading

Aerodynamic drag on an orbiting spacecraft is a significant perturbation source at low Earth orbit. The aerodynamic modeling employed here focuses on simplicity in light of the concept validation emphasis of this study. It is assumed that the incident atmospheric molecules impact the spacecraft without reflection and lose their entire energy upon impact. The shadowing of the flowfield of one part of the spacecraft from another is not considered here. It is further assumed that the component of drag due to the rotation of the spacecraft can be ignored. These are common assumptions for control design purposes.[10]

To apply aerodynamic torque to the unloading of momentum, specific control surfaces on the spacecraft are employed. It is assumed that these control surfaces have the characteristics of flat plates, such as solar panels that might be designed

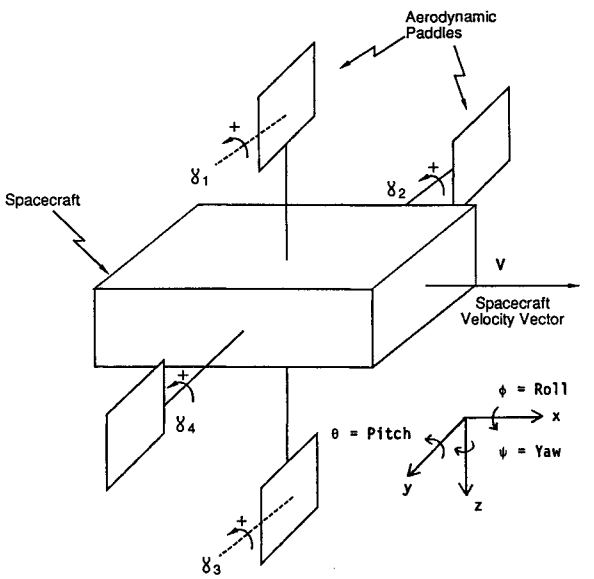

Fig. 2 Aerodynamic unloading paddle configuration.

to serve also as aerodynamic paddles. If there are n such plates, then each plate i will have $\hat{N}_i$ as a unit normal, and r_i can be taken as the vector from the spacecraft center of mass to the center of pressure of plate i. Then the aerodynamic torque arising from the n plates can be expressed in body frame as

$$T_A = -\frac{1}{2}\rho v^2 \left[\sum_{i=1}^{n} C_{Di} A_i \cos\alpha_i r_i\right] \times \hat{v} = \sum_{i=1}^{n} T(\alpha_i)_{Ai} \tag{5}$$

Here α_i is angle of attack on control surface plate i, A_i is area of plate i, C_{Di} is drag coefficient of plate i, ρ is atmospheric density, v is spacecraft velocity, $\hat{v}$ is unit vector in velocity direction, and $T(\alpha_i)_{Ai}$ is the aerodynamic torque due to plate i. Linearizing about $\alpha_i = 0$, Eq. (5) can be approximated for small angles of attack by

$$T_A = \sum_{i=1}^{n} \frac{dT_{Ai}}{d\alpha_i}\alpha_i \tag{6}$$

Expressed in this form, the plate angles of attack α_i are the unloading control variables.

The aerodynamic paddle configuration employed in simulation is shown in Fig. 2. We assume that the distance of each paddle's center of pressure to the spacecraft's center of gravity

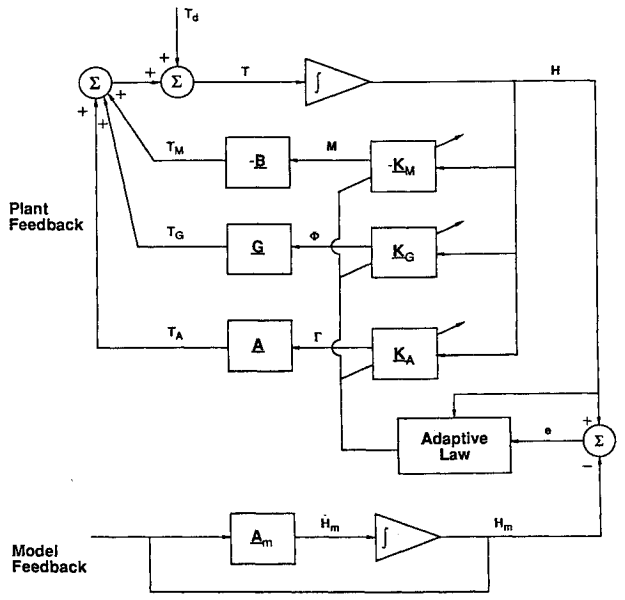

Fig. 3 Adaptive momentum feedback loop.

is $l = 10$ m and the area of each paddle is $A = 5$ m^2. The assumption of a constant drag coefficient in the aerodynamic torque given by Eq. (5) suggests the imposition of a constraint limit on paddle angle fluctuation. A stop of ± 30 deg from the angle set points is assumed for the paddle angles γ_1, γ_2, γ_3, and γ_4. The set points are at an edge-on orientation toward the air flow, which represents a turn angle of 90 deg. Carrying out the partial derivatives of Eq. (6) for the paddle angles γ_i, $i = 1, 4$ depicted in Fig. 2 yields

$$T_A = \underline{A}\Gamma \tag{7}$$

where $\Gamma = [\gamma_1\ \gamma_2\ \gamma_3\ \gamma_4]^T$ and

$$\underline{A} = (l/2)C_D\rho(t)v^2(t)A\begin{bmatrix} 0 & 0 & 0 & 0 \\ -\sin\gamma_1 & 0 & \sin\gamma_3 & 0 \\ 0 & \sin\gamma_2 & 0 & \sin\gamma_4 \end{bmatrix}$$

General Form of Unloading Torques

All of the unloading torques discussed above have the following matrix form

$$T_U = \underline{C}\Upsilon \tag{8}$$

where $U = M$, G, or A, $\underline{C}$ is a coefficient matrix, and Υ is a vector of control variables. The three mechanisms used for momentum control are employed as follows. Magnetic unloading takes place by regulating the current through onboard electromagnets. The generated magnetic dipole M is the control. Gravity gradient unloading occurs when the attitude offset angles roll ϕ and pitch θ are controlled by reference inputs commanded to the attitude control system (ACS). Aerodynamic unloading is controlled by the rotation of paddle appendages through calculated angles γ_1, γ_2, γ_3, γ_4 to create a desired drag torque. These paddles are considered dedicated to the aerodynamic unloading control function in this study and are postulated to have the orientation on the spacecraft body shown in Fig. 2. The change in angular momentum with respect to inertial frame due to T_U is given by

$$\Delta\mathfrak{H}_U = \int_{t_1}^{t_2} T_U^I\, dt \tag{9}$$

where superscript I denotes vectors expressed in inertial frame. An unloading control law seeks a torque T_U such that[3]

$$\Delta\mathfrak{H}_U = -\Delta\mathfrak{H} \tag{10}$$

Adaptive Control Approach

The design of an MRAC scheme to control angular momentum using external spacecraft torques must accommodate several design issues: 1) the time varying nature of the external torques, 2) the momentum bounds determined by wheel saturation limits, 3) the boundedness of the adjusted parameters, and 4) the presence of disturbances (which are assumed to possess known bounds).

Porter and Tatnall[5] describe a multivariable MRAC scheme that is applicable to the momentum unloading problem but lacks discussion on boundedness of the adjusted parameters or performance in the presence of external disturbances. Peterson and Narendra[11] present a bounded error MRAC scheme in the presence of external disturbances. They apply a dead zone method that accommodates aforementioned items 2–4. The idea is to turn off parameter adaptation when the plant state is within a dead zone surrounding the origin. Such a scheme lends itself to a spacecraft onboard computer, which would activate a simple on-off switch to implement the algorithm. The dead zone method is chosen here for its simplicity and effectiveness in this application. In this section, we discuss the implementation of a dead zone procedure for the time varying momentum unloading system.

Control Loop Configuration

The three-way MRAC unloading scheme in this study is modeled as an adaptive feedback system shown in Fig. 3. Controls $M = [M_x\ M_y\ M_z]^T$, $\Phi = [\phi\ \theta]^T$, and $\Gamma = [\gamma_1\ \gamma_2\ \gamma_3\ \gamma_4]^T$ generate torques T_M, T_G, and T_A through environmental interaction. They are regulated by matrix gains $\underline{K}_M = \{k_{Mij}\}$, $\underline{K}_G = \{k_{Gij}\}$, and $\underline{K}_A = \{k_{Aij}\}$, applied to the reaction wheel momentum vector $\underline{H}$. Components of these matrix gains are adjusted by the adaptation laws. The three control torques and disturbance torque T_d constitute the total torque T acting on the spacecraft. T_d represents the total environmental disturbance torque together with the ACS torque, and additionally it is assumed to include other unmodeled disturbance effects. Under the assumption of perfect attitude control, all of the angular momentum imparted to the spacecraft by the resulting torque T is absorbed by the reaction wheels and denoted by H. The total torque T obeys the dynamic equations

$$T = \frac{d^I\mathfrak{H}}{dt} = \frac{d^I H}{dt} \tag{11}$$

where $[d^I(\ )/dt]$ denotes differentiation with respect to inertial frame. The integrator block in Fig. 3 that represents Eq. (11) implies therefore the following: 1) transformation of T from body frame to inertial frame to get T^I, 2) integration of T^I to get H^I according to Eq. (11), and 3) transformation of H^I to body frame to get $H = \mathfrak{H}$. In body frame, Eq. (11) can be written as

$$\dot{H} + \underline{\Omega}H = T \tag{12}$$

where $(\dot{})$ stands for differentiation with respect to body frame, $\omega = [\omega_x\ \omega_y\ \omega_z]^T$ is the angular velocity of body frame with respect to inertial frame, and

$$\underline{\Omega} = \begin{bmatrix} 0 & -\omega_z & \omega_y \\ \omega_z & 0 & -\omega_x \\ -\omega_y & \omega_x & 0 \end{bmatrix}$$

Using Eqs. (2), (4), (7), and (12), we define the state equations of the plant as (see Fig. 3)

$$\dot{H} = (-\underline{\Omega} + \underline{BK}_M + \underline{GK}_G + \underline{AK}_A)H + T_d \tag{13}$$

The model dynamics, represented by the lower block of Fig. 3, are given by

$$\dot{H}_m = \underline{A}_m H_m \tag{14}$$

The constant matrix $\underline{A}_m$, a design parameter, is chosen to be a Hurwitz matrix resulting in an exponentially stable model trajectory $H_m(t)$. Hence, the plant state is to be controlled to follow an exponentially decaying model state. The state error $e \equiv H - H_m$ and plant state H are used to dynamically adjust the gain matrices $\underline{K}_M$, $\underline{K}_G$, and $\underline{K}_A$ using an adaptive law.

Derivation of Adaptive Laws

Consider the dynamics of the system in Fig. 3 in terms of the state error e:

$$\dot{e} = \dot{H} - \dot{H}_m$$

$$= A_m e + (-\underline{\Omega} + \underline{BK}_M + \underline{GK}_G + \underline{AK}_A - \underline{A}_m)H + T_d \tag{15}$$

The system equations given in Eq. (15) will be referred to as the error system. We analyze the stability of this system using the direct method of Lyapunov. Consider an augmented state of the error equation, Eq. (15), to be $[e^T\ A^T]^T$, where A is a 9×1 vector containing the elements of matrix $\underline{\mathfrak{A}} = \{\alpha_{ij}\}$ given by

$$\underline{\mathfrak{A}} = -\underline{\Omega} + \underline{BK}_M + \underline{GK}_G + \underline{AK}_A - \underline{A}_m \tag{16}$$

We choose as a Lyapunov function candidate

$$V = \frac{1}{2} e^T \underline{P} e + \sum_{i=1}^{3}\sum_{j=1}^{3} \nu_{ij}\alpha_{ij}^2 \tag{17}$$

where $\nu_{ij} > 0 \forall i,j$. The matrix $\underline{P}$ is computed from the Lyapunov equation

$$\underline{P}\underline{A}_m + \underline{A}_m^T \underline{P} = -\underline{Q} \tag{18}$$

given the design choices of $\underline{A}_m$ and the constant $\underline{Q} = \underline{Q}^T > 0$. The Hurwitz character of $\underline{A}_m$ ensures that $\underline{P}$ is unique and positive definite.

Differentiation of V yields

$$\dot{V} = \dot{e}^T \underline{P} e + e^T \underline{P} \dot{e} + \sum_{i=1}^{3}\sum_{j=1}^{3} \nu_{ij}\alpha_{ij}\dot{\alpha}_{ij} \tag{19}$$

Expanding Eq. (19), we further obtain

$$\dot{V} = -e^T \underline{Q} e + \sum_{i=1}^{3}\sum_{j=1}^{3} (\nu_{ij}\dot{\alpha}_{ij} + 2h_j e^T P_i)\alpha_{ij} + 2e^T \underline{P} T_d \tag{20}$$

where h_j is the jth component of the vector H and P_i is the ith column of the matrix $\underline{P}$. To assure stability (or boundedness) in the sense of Lyapunov, we desire Eq. (20) to be at least negative semidefinite. Thus we let

$$\dot{\alpha}_{ij} = -\delta_{ij} h_j e^T P_i \tag{21}$$

where $\delta_{ij} = 2/\nu_{ij}$ are redefined constants. Equation (21) is the adaptive law of the system. Substituting Eq. (21) into Eq. (20) produces the Lyapunov function derivative

$$\dot{V} = -e^T \underline{Q} e + 2e^T \underline{P} T_d \tag{22}$$

This stability analysis is carried out by first treating the system of Eq. (15) as if it were unperturbed (had no T_d term). Disturbance considerations are discussed in the next subsection. Assuming $T_d = 0$, Eq. (22) becomes

$$\dot{V} = -e^T \underline{Q} e \tag{23}$$

The discussion that follows contains a number of results that are stated here without proof. The proofs are given in Burns[12] and are based on the analyses of Yoshizawa,[13] LaSalle and Lefschetz,[14] and others (see Burns[12] for a complete reference list).

Consider the error system in Eq. (15) under the adaptive law given in Eq. (21). Assume that $T_d = 0$, i.e., no disturbances are present. Then we have the following results:

Result 1: The equilibrium $[e^T\ A^T]^T = 0$ is uniformly stable.

Result 2: The solutions of the error system are uniformly bounded.

Result 3: The error component of the state e satisfies

$$\lim_{t \to \infty} e = 0$$

Proof of result 3: Since e and the elements of $\underline{\mathfrak{A}}$ are bounded, V is bounded from above [see Eq. (17)], as well as from below, because $V \geq 0$. Hence

$$\int_0^t \dot{V}\, dt = V(t) - V(0) \tag{24}$$

which implies that

$$\int_0^t e^T \underline{Q} e\, dt = V(0) - V(t) \tag{25}$$

Hence

$$\int_0^\infty e^T \underline{Q} e\, dt = V(0) - V(\infty) < \infty \tag{26}$$

Consider Eq. (15), with $T_d = 0$. It is clear that H is bounded because of the boundedness of e and the exponential stability of H_m. Since $\underline{A}$, e, and $\underline{A}_m$ are bounded, this implies that $\dot{e}$ is bounded, hence e is uniformly continuous. From this fact and Eq. (26), we conclude that $e(t) \to 0$ as $t \to \infty$. Q.E.D.

Results 1-3 thus establish that for the undisturbed system, the adaptive parameters are uniformly bounded and the angular momentum H approaches the model H_m as time increases under the adaptive control law $\dot{\alpha}_{ij} = -\delta_{ij} h_j e^T P_i$.

Consideration of Disturbances

It is important to extend the analysis of the previous subsection to account for the presence of the disturbance T_d in the adaptive system represented by Eq. (15) and Fig. 3. A dead zone technique similar to the one described by Peterson and Narendra[11] is employed to develop adaptation laws accounting for T_d. The idea is to modify the adaptive law so that when the trajectory of the state e falls within a preset region surrounding the origin, parameter adaptation is ceased. This added feature prevents adaptation in a situation where the right side of Eq. (22) may become positive, which would indicate stability uncertainty of the error system.

The adaptive law given by Eq. (21) is modified to be the following:

$$\dot{\alpha}_{ij} = \begin{cases} -\delta_{ij} h_j e^T P_i, & \|e\| > 2\dfrac{\|\underline{P}\|_i D_0}{\|\underline{Q}\|_i} \\ 0, & \|e\| \leq 2\dfrac{\|\underline{P}\|_i D_0}{\|\underline{Q}\|_i} \end{cases} \tag{27}$$

where D_0 is an upper bound on the disturbances such that $D_0 \geq \|T_d\|_{\max}$, and $\|\underline{P}\|_i$ and $\|\underline{Q}\|_i$ are the induced matrix

norms of $\underline{P}$ and $\underline{Q}$, respectively. The Lyapunov function conditions are now the following:

1) $V > 0$

2) $\dot{V} \leq 0$, $\|e\| > 2(\|\underline{P}\|_i D_0 / \|\underline{Q}\|_i)$

These reduced Lyapunov function attributes result in less stringent stability characteristics than the undisturbed system analyzed in the previous subsection. However, the goals of this application are to maintain subsaturation bounds on angular momentum H and finite bounds on adaptive parameters $\underline{K}_M$, $\underline{K}_G$, and $\underline{K}_A$. To achieve these goals, we apply the concepts of ultimate boundedness and practical stability discussed by LaSalle and Lefschetz[14] defined in the following.

Definition (Ultimate Boundedness)

A system $\dot{x} = F(t,x)$ is ultimately bounded if there is a $b > 0$ such that corresponding to each solution $x(t)$ of the system, there is a $T > 0$ with the property that $\|x(t)\| < b$ for all $t > T$.

Definition (Practical Stability)

Given an unperturbed system $\dot{x} = F(x,t)$, $t \geq 0$ and a perturbed system $\dot{x} = F(x,t) + p(x,t)$, $t \geq 0$, where $F(0,t) = 0$ and $p(x,t)$ represents a perturbation. Given also a number δ and two sets Q and Q_0, where Q is a closed and bounded set containing the origin and Q_0 is a subset of Q. Let P be the set of all perturbations p satisfying $\|p(x,t)\| \leq \delta$ for all $t \geq 0$ and all x. If for each initial state x_0, each p in P, and each $t_0 \geq 0$, the solutions to the perturbed system are in Q for all $t \geq 0$, the origin is said to be practically stable.

Consider the error system in Eq. (15) with $T_d \neq 0$ and an adaptation law given by Eq. (27). Then applying the above definitions we have the following results:

Result 4: The state $[e^T \; A^T]^T$ of the error system is ultimately bounded.

Result 5: The error system is practically stable.

Result 5 provides us with an upper bound for the solutions of the adaptive momentum system which is a function of the system disturbances and the physical characteristics of the spacecraft. This analysis is further supported by an argument about the behavior of the trajectories of the system given by Eq. (15) as they pass in and out of the dead zone. We have shown earlier that outside of the dead zone, $\dot{V} \leq 0$. Thus V is nonincreasing, implying that the state $[e^T \; A^T]^T$ is inhibited from diverging from the origin [see Eq. (17)]. Inside the dead zone, adaptation is switched off [Eq. (27)] indicating that $\underline{\Omega}$ will not grow, and (by definition) e is confined to that region. Thus e tends toward the dead zone region.

In summary, it is demonstrated that the perturbed adaptive momentum unloading system represented by Eq. (15) and Fig. 3 is ultimately bounded and practically stable. As a result, we can say that the reaction wheel momentum H remains bounded and in the vicinity of the dead zone. The dead zone can be thought of as an attractive set to the trajectory of H. It serves as a region of nonadaptation to accommodate the presence of bounded disturbances and also as a region of periodic momentum fluctuation in which we are not interested for the practical purposes of unloading.

Implementation of Adaptive Law

In the following, we consider the case for which $\underline{\Omega}$ is a constant matrix. This is the case in inertial configurations, or in circular orbits in Earth-pointing configuration when neglecting Earth motion and nodal regression. Substituting Eq. (16) into Eq. (21) and denoting $\{\cdot\}$ to mean "the matrix whose elements are . . . ," we obtain the adaptation equation

$$\underline{B}\dot{\underline{K}}_M + \underline{G}\dot{\underline{K}}_G + \underline{A}\dot{\underline{K}}_A = -\dot{\underline{B}}\underline{K}_M - \dot{\underline{A}}\underline{K}_A - \{\delta_{ij} h_j e^T P_i\} \quad (28)$$

which can be written as

$$\underline{X}\dot{\underline{K}} = R \quad (29)$$

where $\dot{\underline{K}}$ is a 27-element column matrix containing $\dot{k}_{Mij}$, $\dot{k}_{Gij}$, and $\dot{k}_{Aij}$, $i,j = 1, 2, 3$; $\underline{X}$ is a sparse 9×27 matrix; and R is a 9-element vector containing all the terms of the right side of Eq. (28). Since $\underline{X}$ is of rank 9, only 9 parameter derivatives of 27 total elements are selected for adaptation; the remaining 18 elements are set to zero. The selection process, described in detail in Burns,[12] is driven by the requirement that all three orthogonal directions in the spacecraft body frame be viable for unloading by at least one of the three unloading sources employed.

Design Parameters of the Adaptive System

Given the stability analysis of the previous subsections, there exists a number of design parameters that are available to fine tune the system for a particular spacecraft configuration. These include the MRAC model dynamics matrix $\underline{A}_m$, the positive definite symmetric matrix $\underline{Q}$, the system disturbance upper bound D_0, and the adaptive gains δ_{ij}.

The approach taken for selecting the design parameters is to first choose D_0 and $\underline{Q}$. D_0 is chosen to be at the maximum possible absolute value that T_d may physically attain. The matrix $\underline{Q}$ is used to shape the speed or "strength" of the closing of the error between H and H_m [see Eq. (22)]. Next consult Eq. (27) to obtain the desired ratio $\|\underline{P}\|_i / \|\underline{Q}\|_i$ from the desired size of the dead zone, which determines the matrix $\underline{P}$. The desired dead zone is sized to the magnitude of momentum below which the fluctuations are not important, for example one-fourth the saturation limit of wheel momentum H. Then Eq. (18) can be employed to calculate the value of $\underline{A}_m$. The choices of D_0, $\underline{Q}$, and $\underline{A}_m$ thus provide influence over the speed of control on e. The values of adaptive gains δ_{ij} are chosen to influence the speed of adaptation of the parameter matrices $\underline{K}_M$, $\underline{K}_G$, and $\underline{K}_A$.

Simulation Studies

System Models

The momentum unloading algorithms presented in this study are validated via orbit simulation. The following models are employed.

Magnetic Field Model

The magnetic model used for unloading algorithm verification represents an undistorted, steady-state field that does not account for temporal variations due to short period solar activity (magnetic storms) or near-Earth anomalies. A tilted dipole model is chosen for its simplicity and general acceptance for magnetic unloading algorithm design.[12,15,16]

Environmental Perturbation Torque Model

Environmental perturbation torques are dominated in low Earth orbit by aerodynamic drag fluctuating on a cyclical basis with the orbital period. Keeping with the simplicity of a concept validation model, the following is chosen to represent the perturbation torque (body coordinates):

$$T_{abx} = 0$$

$$T_{aby} = -A_y \sin\omega_0 t - S_y$$

$$T_{abz} = A_z \sin\omega_0 t + S_z \quad (30)$$

where ω_0 is orbit rate and A_y, A_z, S_y, S_z are constant coefficients whose values are determined by estimating aerodynamic drag characteristics from previously established models depending on the orbit being simulated.[3,10] Due to the Earth-pointing attitude assumption, $T_{abx} = 0$.

Atmospheric Density Model

The atmospheric density model employed for aerodynamic torque control via paddles is a sinusoid which takes into

Table 1 Properties of small spacecraft in simulation[9]

Principal moments of inertia, kg-m^2	
I_x	125
I_y	116
I_z	135
Reaction wheel saturation limits, N-m-s	
$H_{x\max}$	± 5
$H_{y\max}$	± 5
$H_{z\max}$	± 5
Magnetic torquer maximum moments, amp-m^2	
$M_{x\max}$	± 50
$M_{y\max}$	± 50
$M_{z\max}$	± 50

Table 2 Properties of large spacecraft (Gamma Ray Observatory) in simulation

Principal moments of inertia, kg-m^2	
I_x	50,760
I_y	79,550
I_z	95,260
Reaction wheel saturation limits, N-m-s	
$H_{x\max}$	± 200
$H_{y\max}$	± 200
$H_{z\max}$	± 200
Magnetic torquer maximum moments, amp-m^2	
$M_{x\max}$	± 1800
$M_{y\max}$	± 1800
$M_{z\max}$	± 1800

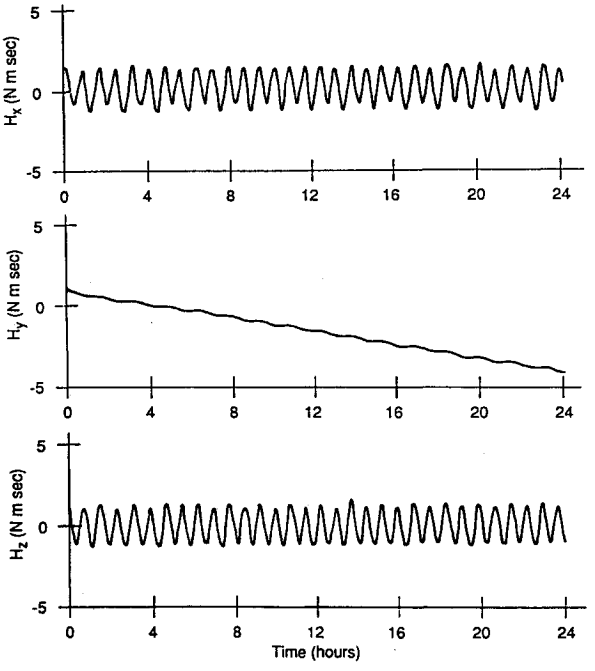

Fig. 4 Small spacecraft momentum without unloading.

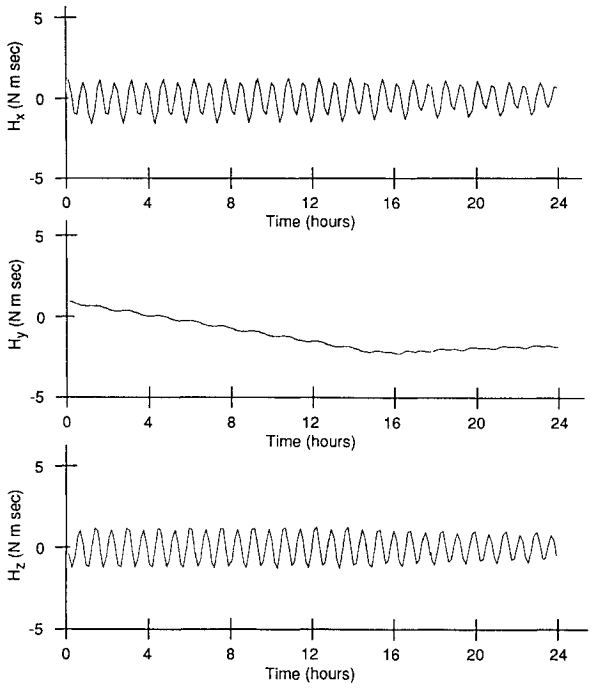

Fig. 5 MRAC, small spacecraft: momentum.

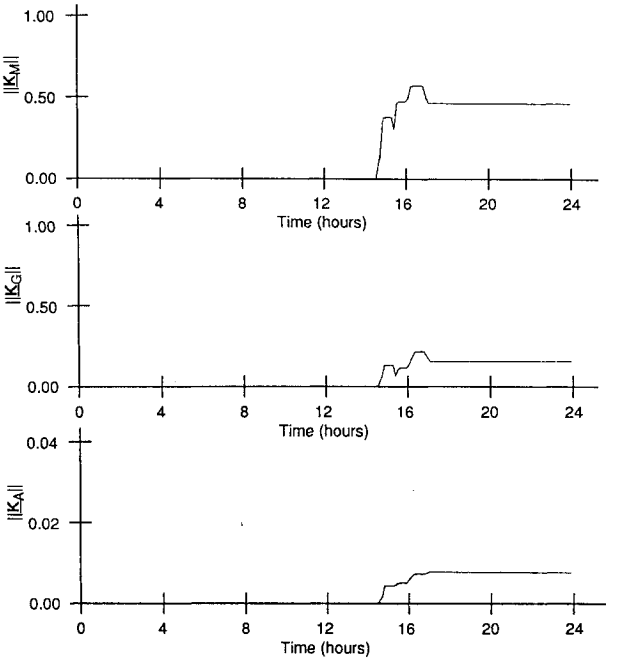

Fig. 6 MRAC, small spacecraft: adaptive parameters.

account the relative fluctuations from night side of the Earth to day side.[10,17] The density model is

$$\rho(t) = \rho_a \sin\omega_0 t + \rho_c \tag{31}$$

where ω_0 = spacecraft orbital rate. For maximum sunspot activity[17] $\rho_a = 4.34 \times 10^{-12}$ kg/m^3 and $\rho_c = 13.46 \times 10^{-12}$ kg/m^3.

Spacecraft Attitude Dynamics and Control Models

The spacecraft dynamics and control models are based on the assumptions of Earth-pointing desired attitude and small attitude angles and angle rates. These models establish the attitude control loop of Fig. 1. The most common attitude controller chosen in this type of problem is a proportional/rate control law. This type of law is chosen, including uncoupling terms, similar to the controllers chosen by Junkins et al.[9] and Shain and Spector.[1] See Burns[12] for a detailed description of the attitude control law employed.

Spacecraft Orbit Simulation Configurations

The orbit simulations performed for validation of the momentum unloading algorithm of this study model a circular

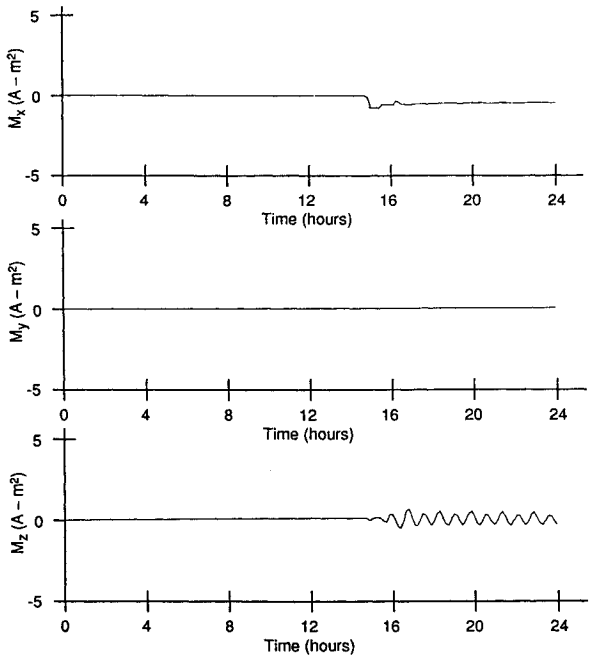

Fig. 7 MRAC, small spacecraft: magnetic moments.

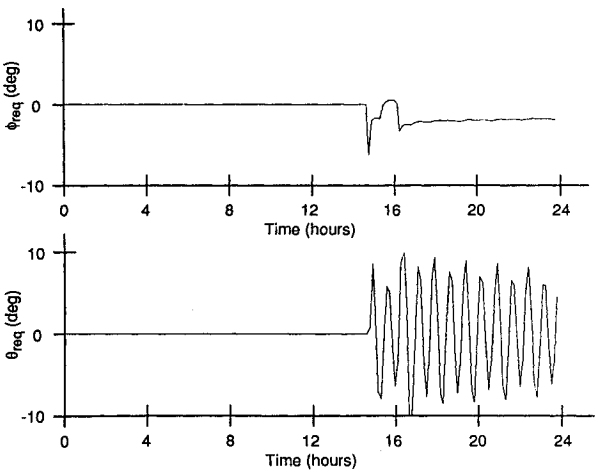

Fig. 8 MRAC, small spacecraft: attitude offset angle control commands.

orbit of altitude 200 n.mi. and inclination 28.5 deg in the Earth-pointing desired attitude. The unloading algorithm is simulated in conjunction with two example spacecraft: a small spacecraft,[9] and a large spacecraft with the properties of the NASA Gamma Ray Observatory (GRO). The principal moments of inertia, angular momentum saturation limits, and magnetic torquer moment limits of the small and large spacecraft are summarized in Tables 1 and 2, respectively.

Simulation Results

Simulation plots given in this study are in spacecraft body coordinates. For a near 90-min spacecraft orbit and a tilted dipole magnetic field simulation model, the magnetic field in spacecraft body coordinates is essentially periodic with a 24-h period. Thus a 24-h simulation provides a complete picture of the adaptive unloading system. The MRAC model H_m that is tracked by wheel momentum H during adaptive unloading is an exponentially decaying vector function whose dynamics are given by Eq. (14). The choice of a diagonal matrix with elements -0.001, -0.002, -0.003 for $\underline{A}_m$ is assumed. The initial conditions of H_m are set equal to the initial conditions of H for the simulation.

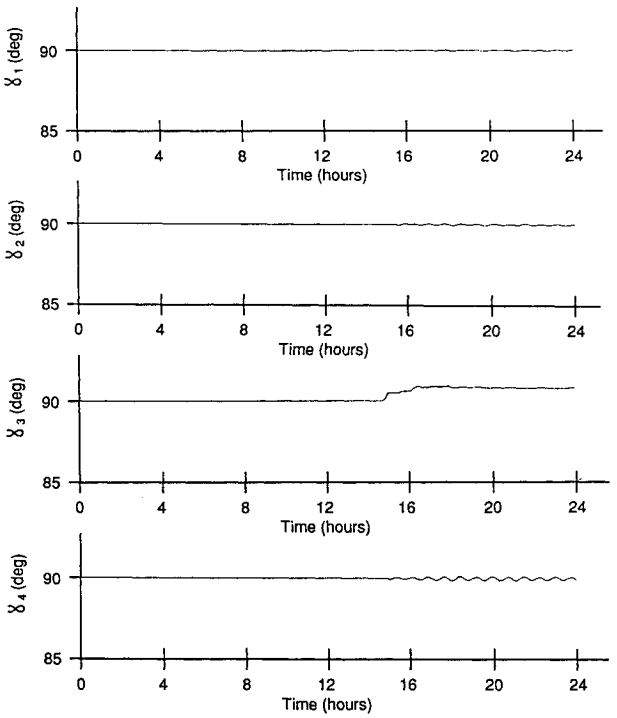

Fig. 9 MRAC, small spacecraft: aerodynamic paddle angles.

Small Spacecraft

The environmental perturbation torque model is given by Eq. (30) with $A_y = 8.6 \times 10^{-5}$, $S_y = 5.7 \times 10^{-5}$, $A_z = 4.3 \times 10^{-4}$, and $S_z = 2.85 \times 10^{-4}$. Simulation characteristics of the small spacecraft without momentum unloading are shown in Fig. 4. It is seen that the secular term magnitude of the momentum y component increases steadily. The objective is to maintain this component bounded well within the saturation limits of ± 5 N-m-s while not adversely affecting the other H components or attitude angles. Note, however, that attitude angle pointing requirements are assumed to be accommodating to the attitude angle variations commanded by the gravity gradient unloading portion of the MUCS. The effect of three-way adaptive unloading for the small spacecraft is illustrated in Figs. 5-9, which depict wheel momentum plots, adaptive parameters, magnetic control moments, attitude offset angle requests, and paddle turn angles, respectively. The adaptive parameter matrices $\underline{K}_M$, $\underline{K}_G$, and $\underline{K}_A$ are presented in terms of the root sum square of all of their elements. The atmospheric density model given by Eq. (31) is set at 10% of sunspot maximum values, which is a near-worst case setting for aerodynamic paddle torque control.

From Figs. 5 and 6 it is clear that momentum magnitude increases in y component until not quite 15 h, when the dead zone is exceeded, signified by the changing of $\underline{K}_M$, $\underline{K}_G$, and $\underline{K}_A$. Adaptation continues for less than 2 h more, after which the y component goes back into the dead zone for the duration of the run. When adaptation is not taking place, $\underline{K}_M$, $\underline{K}_G$, and $\underline{K}_A$ remain constant. The three magnetic control commands, plotted in Figs. 7-9, begin responding when the momentum violates the dead zone boundary. The attitude offset requests shown in Fig. 8 are seen to fit properly within the $\pm$ 10-deg stop limits. The magnetic control moments (Fig. 7) are well within their limits of $\pm$ 50 amp-m^2 (see Table 1). The presence of the y component of magnetic moment control at identically zero is the result of the choice of the nine adaptive parameter elements, discussed previously. The configuration chosen, based on the requirement to provide unloading in all three axes, contains no elements in the second row of $\underline{K}_M$. Paddle angles (Fig. 9) are also well within their stop values.

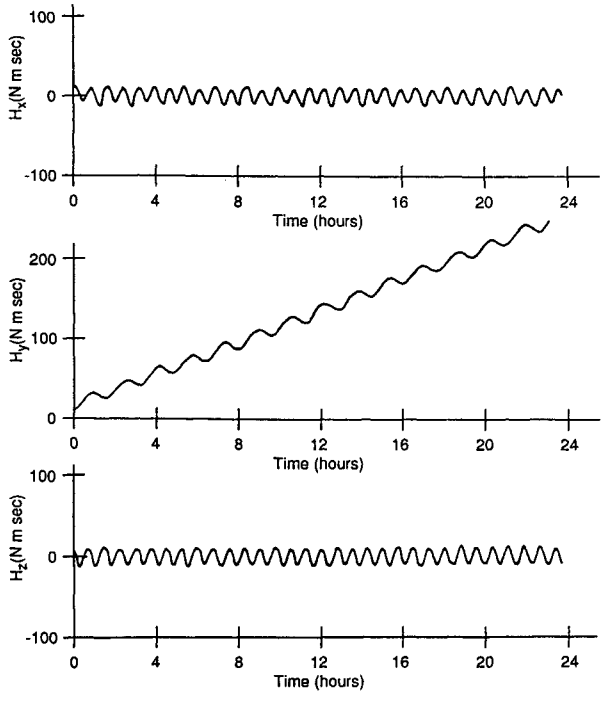

Fig. 10 Large spacecraft momentum without unloading.

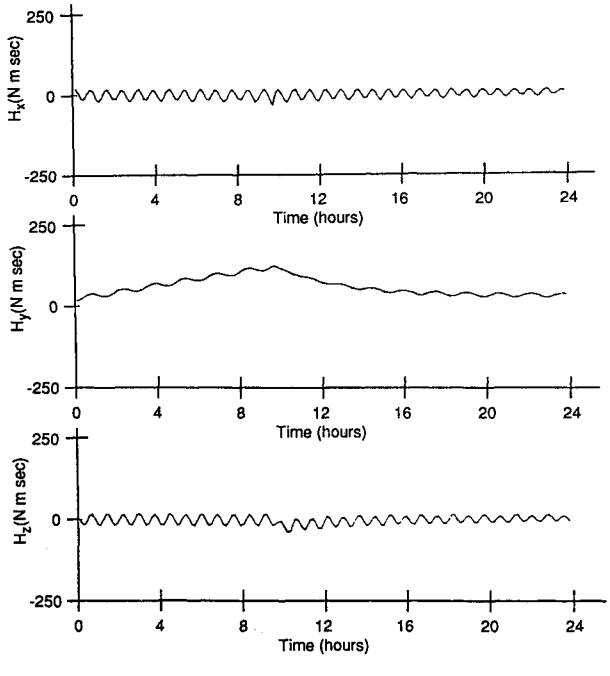

Fig. 11 MRAC, large spacecraft: momentum.

Large Spacecraft

The environmental perturbation torque model is given by Eq. (30) with $A_y = -8.5 \times 10^{-3}$, $S_y = -2.75 \times 10^{-3}$, $A_z = 4.25 \times 10^{-3}$, and $S_z = 1.375 \times 10^{-3}$. Orbit simulation results of the large spacecraft without momentum unloading are shown in Fig. 10. Figure 10 shows the secular term of the y component magnitude of wheel momentum steadily increasing. Adaptive momentum unloading applied to the large spacecraft is illustrated in Fig. 11. The atmospheric density model supporting aerodynamic paddle torque control uses average sunspot activity values for the 370-km altitude.[17] This results in the parameters of Eq. (31) being $\rho_a = 3.25 \times 10^{-12}$ kg/m^3 and $\rho_c = 7.23 \times 10^{-12}$ kg/m^3. Figure 11 shows reaction

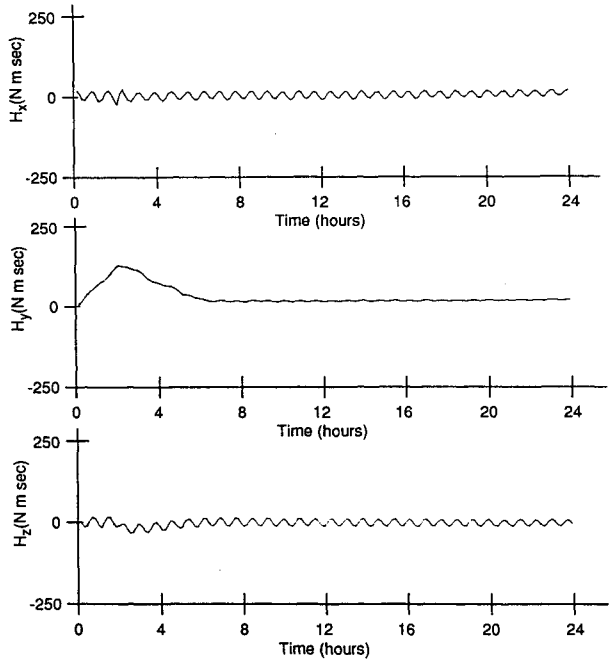

Fig. 12 MRAC, large spacecraft, large disturbance: momentum.

wheel momentum variations of a similar pattern as observed for the small spacecraft. The y component rises out of the dead zone, prompting adaptation. The adaptation lasts less than one orbit's duration, after which the momentum tends toward a periodic steady state within the dead zone.

A further orbit simulation with the large spacecraft is made with a more persistent external perturbation function, given by the following:

$$T_{abx} = 0$$

$$T_{aby} = 0.0055 \sin\omega_0 t + 0.017$$

$$T_{abz} = 0.00275 \sin\omega_0 t + 0.0085 \qquad (32)$$

Equation (32) represents a perturbation torque having a maximum absolute value of twice the torque of the previous cases and constant terms more than six times higher. Thus the secular term of wheel momentum is driven at a much higher rate. The density model supporting aerodynamic torque unloading is given the parameters of maximum sunspot activity, delineated in conjunction with Eq. (31), in accordance with the very high perturbation torque. Figure 12 depicts the results of the large spacecraft orbit simulation with high perturbations. Comparison of Figs. 11 and 12 reveals the more powerful tendency of the y component of H to rise unconstrained when subject to a much higher secular external perturbation. It was found that the adaptive system nonetheless reacts with the familiar pattern of a relatively brief period of adaptation followed by convergence of momentum to a tightly bound steady state. The control effort responses for both large spacecraft cases were found to be very similar in character to the small spacecraft cases. The requirement of ± 1800 amp-m^2 for magnetic control, ± 10 deg for attitude offset control, and ± 30-deg excursions for aerodynamic control were all met.

Conclusion

Three environmental torques were used in combination for the first time in an adaptive control law that demonstrated maintenance of momentum within desired bounds. The method was simulated on two separate model spacecraft possessing widely different mass properties. The judicial use of the dead zone was shown to make adaptive control an appealing method for momentum unloading. The reaction wheel

momentum was allowed to fluctuate within a subset of its saturation limits (the dead zone), only requiring control adjustment when violating that subset. It was shown that the adaptation of system parameters was so efficient that in each simulation, the wheel momentum did not violate the dead zone after the initial episode of adaptation lasting less than one orbit's duration. It is regarded that these results fulfill the goal of this study of concept validation of the adaptive control technique.

Future studies may focus on potential improvements to the presented techniques. A multisource adaptive unloading controller could benefit from a feature to prescribe the ratio of incorporation of the various sources. Also, alternate forms of the adaptive control algorithm could be explored, such as the introduction of auxiliary signals or filters to guarantee greater robustness features. In addition, future studies devoted to specific missions will require that the algorithm be simulated using the most accurate available gravitational, aerodynamic, and magnetic field models. Since spacecraft momentum fluctuates slowly, large time steps are feasible for the implementation of the adaptive unloading scheme, which would facilitate its incorporation into an onboard processor. Sizing and timing studies of such a processor are further tasks for the future.

References

[1]Shain, E. B., and Spector, V. A., "Adaptive Torque Equilibrium Control of the Space Station," AIAA Paper 85-0028, Jan. 1985.

[2]Woo, H. H., Morgan, H. D., and Falangas, E. T., "Momentum Management Concepts for a Space Station," AIAA Paper 86-2047, Aug. 1986; see also Woo, H. H., Morgan, H. D., and Falangas, E. T., "Momentum Management and Attitude Control Design for a Space Station," *Journal of Guidance, Control, and Dynamics,* Vol. 11, No. 1, 1988, pp. 19–25.

[3]Decanini, J. H., Flashner, H., and Schmeichel, H., "Magnetic Control and the 25 kW Power System," American Astronomical Society, AAS Paper 81-004, Feb. 1981.

[4]Camillo, P. J., and Markley, F. L., "Orbit-Averaged Behavior of Magnetic Control Laws for Momentum Unloading," *Journal of Guidance and Control,* Vol. 3, No. 6, 1980, pp. 563–568.

[5]Porter, B., and Tatnall, M. L., "Performance Characteristics of Multi-Variable Model-Reference Adaptive Systems Synthesized by Lyapunov's Direct Method," *International Journal of Control,* Vol. 10, No. 3, 1969, pp. 241–257.

[6]Narendra, K. S., and Valavani, L. S., "Stable Adaptive Control Design-Direct Control," *IEEE Transactions on Automatic Control,* Vol. AC-23, No. 4, Aug. 1978, pp. 570–583.

[7]Narendra, K. S., "Stable Identification Themes," *System Identification, Mathematics in Science and Engineering,* Vol. 126, Academic, New York, 1976, pp. 165–209.

[8]Ioannou, P. A., and Kokotovic, P. V., "Instability Analysis and Improvement of Robustness of Adaptive Control," *Automatica,* Vol. 20, No. 5, 1984, pp. 583–594.

[9]Junkins, J. L., Rajaram, S., Baracat, W. A., and Carrington, C. K., "Precision Autonomous Satellite Attitude Control Using Momentum Transfer and Magnetic Torquing," *The Journal of the Astronautical Sciences,* Vol. XXX, No. 1, 1982, pp. 31–48.

[10]"Spacecraft Aerodynamic Torques," NASA Space Vehicle Design Criteria, NASA SP-8058, Jan. 1971.

[11]Peterson, B. B., and Narendra, K. S., "Bounded Error Adaptive Control," *IEEE Transactions on Automatic Control,* Vol. AC-27, No. 6, Dec. 1982, pp. 1161–1168.

[12]Burns, T. F., "Angular Momentum Unloading of Spacecraft Utilizing the Earth Environment," Ph.D. Dissertation, Dept. of Aerospace Engineering, Univ. of Southern California, Los Angeles, CA, Aug. 1988.

[13]Yoshizawa, T., *Stability Theory by Lyapunov's Second Method,* Mathematical Society of Japan, Tokyo, 1966, pp. 1–4, 27–51.

[14]LaSalle, J., and Lefschetz, S., *Stability by Lyapunov's Direct Method with Applications,* Academic, New York, 1961, pp. 116–126.

[15]McElroy, T. T., "Attitude Determination and Control of a Spinning Satellite Using the Earth's Magnetic Field," Ph.D. Dissertation, Dept. of Electrical Engineering, Univ. of Michigan, Ann Arbor, MI, June 1973.

[16]Eller, T. J., and Wagie, D. A., "Earth's Magnetic Field Models for Dumping Momentum Magnetically on GPS Satellites," *Journal of Guidance, Control, and Dynamics,* Vol. 5, No. 9, 1982, pp. 438–441.

[17]Valley, S. L. (ed.), *Handbook of Geophysics and Space Environments,* McGraw-Hill, New York, 1965, pp. 3-37–3-42.